Journal of Computer Science and Artificial Intelligence
ISSN: 3078-8242 (Print), ISSN: 3078-2309 (Online) | Vol. 9, No. 2, 2026

A Convex-Hull and Robust Expected-Optimization Framework for Bearing-Only Localization and Source Removal

Zhitong Zhu *, Zirui Huang, Sicong Li

Nanjing Forestry University, Nanjing, China

* **Corresponding author**: (Email: zhuzhitong@njfu.edu.cn)

Abstract: Bounded bearing error forces a mobile agent to localize stationary sources and remove them without range measurements and without knowing how many exist. Four computations are chained into one executable framework. Angular sectors from successive bearings intersect the target disk into a feasible set, a Graham scan rebuilds it as a convex hull, and rotating calipers cut the diameter search to $O(m)$; a triangle and a rectangle show that the disk on that diameter does not certify coverage, which is therefore tested vertex by vertex. A three-state diameter loss, area-weighted by polar cells and enveloped over the unknown reception radius, is minimized lexicographically under a guaranteed success rate, giving 1087.25 m, ±30.15°, 59.941 m and 0.9899, which is 25.46% below the initial scheme. Six outer stations plus the origin satisfy an analytic covering condition, the ring radius is set at 1400 m just right of the Pareto knee, with the worst position 913.91 m from a station, and removal order is solved by open-route dynamic programming within a rolling horizon. Directional sources are handled by a half-plane approach rule and an outer polygon screened by a Clopper–Pearson bound. Simulated per-source time rises with dispersion, with a fitted slope of 0.08172 and $R^2 = 0.9914$. The framework turns bounded measurements into a verifiable feasible set, a candidate region and a removal sequence.

Keywords: Convex Hull, Robust Optimization, Coverage Search, Rolling-Horizon Scheduling.

1. Introduction

A mobile agent that reports only a bearing must find stationary sources in a bounded region and remove them once close enough. Three uncertainties act at once: the reading has finite precision, so one observation confines the source to an angular sector and only an intersection of several yields a usable position set; the distance cannot be measured, and a further reading is available only inside the reception range; the source count is unknown, so the moment to stop searching must rest on whether coverage is sufficient.

Geometry governs accuracy when only bearings are available: uncertainty shrinks as the intersection angle approaches a right angle and as the baseline becomes more lateral to the line of sight, with the best layout shifting as ranges change [1], and error lower bounds refine the picture from the estimator side [2]. Active localization of intermittent emitters couples discovery, approach and confirmation in an online policy [3]. Such work answers where to stand in order to estimate well and leaves the question of when removal is safe outside the estimator.

When the error is bounded the object of interest is the feasible set, which set-membership estimation returns as a provably containing set updated by intersection [4]. Decisions then rest on its extreme features, how wide the region is and whether a disk of the removal radius encloses it, and these are usually replaced by volume or ellipsoidal approximations.

Coverage search organizes discovery around sweep paths and coverage ratios [5]; directional sensor networks match node orientation against coverage and place nodes by swarm intelligence [6, 7]; multi-platform allocation splits discovery and handling into assignment and sequencing [8]. These studies assume an isotropic detection radius, leave the source count out of termination and use bearings only as an accuracy correction, so the assumption fails once a source radiates forward.

Four computations are chained here. Angular intersection yields the feasible set, and the hull with rotating calipers yields its diameter with a coverage test, the common interface for later criteria. A three-state loss, an area-weighted prior and a worst-case envelope over the radius interval produce the second station, with reliability imposed as a hard constraint. A seven-point equiangular structure with coverage-exclusion screening binds discovery to termination, while the enclosing circle and open-route dynamic programming bind removal to sequencing. Directional sources take an outer polygon and a half-plane rule. What passes between the segments is one object in successive forms: the feasible set, two scalars read off it, and the action sequence.

The verification instance is the screening of radio interference sources in a disk of radius 1800 m, with 10 to 16 of 20 bands occupied, a reception radius between 1000 m and 1500 m, a bearing error within ±1°, a speed of 5 m/s, 5 s per measurement, 1 s per band switch and 5 s for confirmation plus removal within 20 m. The instance fixes the numbers, not the method: only the angular half-width, the radius interval, the removal distance and four action durations enter the model. Sources are taken as mutually non-interfering and stationary, processing time as negligible and the detector as level with the source. The main contributions are as follows:

A hull reconstruction and rotating-calipers diameter algorithm reducing the search to linear time, with two instances showing that the diameter disk is not a coverage certificate, so accuracy and removability become separate criteria.

A three-state diameter loss, area-weighted and enveloped over the radius interval, solved lexicographically under a

guaranteed success rate, yielding the second station and a near-optimal region.

An analytic seven-point covering structure with a Pareto-knee ring radius, coverage-exclusion screening, an enclosing-circle removal test, dynamic programming and a rolling horizon on one time scale.

An angular coverage criterion with a proof of the outward tangential blind zone, from which joint inner-outer detection is built and screened by a confidence lower bound.

2. Bounded-Error Localization Region and Its Diameter

2.1. Angular Intersection and Feasible Set

With a bounded, non-random error a single observation corresponds not to a ray but to an angular sector. Let the i-th detection point be $S_i = (x_i, y_i)$ with measured bearing θ_i and error bound $\delta = 1^\circ$; the admitted positions are

$$D_i = \left\{ x : \left| \arg(x - S_i) - \theta_i \right| \le \delta, \| x - S_i \| \le R \right\} \quad (1)$$

Where the distance bound is the largest reception radius. With the target disk $\Omega = \{(x, y) : x^2 + y^2 \le 1800^2\}$ and every observation imposed at once, the feasible set is

$$F = \Omega \cap \bigcap_{i=1}^{n} D_i \quad (2)$$

Sectors and disk are convex and so is their intersection, hence F is a bounded convex polygon with at most $2n+1$ edges. Figure 1 shows the contraction under three sequential observations: the second narrows the region appreciably and the third presses it close to the source. The boundary is fixed by pairwise intersections of sector edges, not by a single angular width, so the diameter must be computed over vertex pairs.

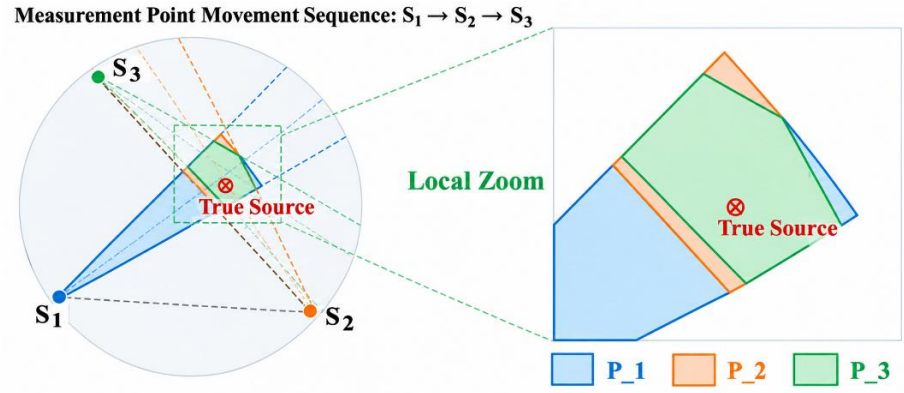

Figure 1. Contraction of the feasible set under three sequential observations, with a magnified view

Candidate vertices come from pairwise intersections of boundary lines, each substituted back into all constraints, and the survivors are ordered by a Graham scan about the lowest point, popping clockwise triples until counter-clockwise order holds [9]; tolerances follow the coordinate scale, a relative 10^{-6} m separating collinear from near-collinear triples at coordinates of order 10^3 m. Interior points cannot contribute to the diameter: if a farthest point lies inside an edge, moving along that edge towards an end point leaves the distance to the opposite point no smaller, so a continuous extremal problem over a region becomes a finite one over vertices.

2.2. Rotating-Calipers Diameter

Vertex enumeration compares $m(m-1)/2$ pairs at cost $O(m^2)$. A convex polygon attains its diameter at an antipodal pair, two vertices touched by the same pair of parallel supporting lines. With the current edge $V_i V_{i+1}$ and a candidate V_j opposite, twice the triangle area decides whether the candidate advances, a larger value meaning a larger perpendicular distance; once the area stops increasing the antipode is recorded. The edge rotates over the boundary while the antipode index advances monotonically, so each vertex is visited a constant number of times and the cost is $O(m)$.

Distances are compared as squares, so no square root is needed during traversal.

2.3. Diameter-Circle Coverage Test

A diameter bounds the distance between two points of the region, which is not the same as one disk enclosing it. Taking the farthest pair as diameter with midpoint O and radius $D/2$, the region is covered exactly when every vertex P_i satisfies $\| P_i - O \| \le D/2$, and since both polygon and disk are convex, vertices inside the disk put the whole polygon inside.

Two instances settle the question. For the triangle $A = (-1, 0)$, $B = (1, 0)$, $C = (0, \sqrt{3})$ the farthest pair is A, B with $|AB| = 2$, the disk on AB has radius 1, and C lies at $\sqrt{3} > 1$ from the centre, so the disk misses part of the region. For the rectangle with corners $(\pm 1, \pm 1)$ the farthest pair are opposite corners at $2\sqrt{2}$ and the other two lie exactly on that circle, so coverage holds. Figure 2 places the two side by side.

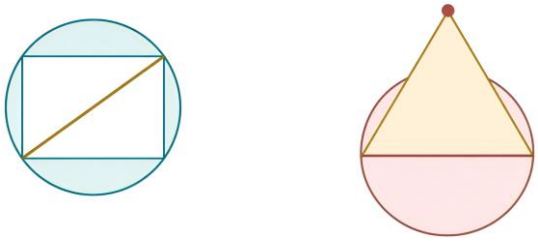

Figure 2. Two instances deciding whether the disk on the farthest vertex pair covers the feasible set

The test must therefore run separately from the diameter: a small diameter says the region is narrow, not that a removal disk encloses it. The removal condition concerns the minimum enclosing radius, which in the triangle differs from half the diameter by about 15%, enough near a removal distance of 20 m to reverse the answer.

3. Robust Expected Optimization of the Second Station

The measured bearing supplies a reference direction, so the next station is fixed by the baseline length and the relative offset.

3.1. Baseline Parameterization and Three-State Loss

With the first detection point at the origin, first measured bearing $\hat{\theta}_1$, bearing error η and source range ρ, the source sits at $\rho u(\hat{\theta}_1+\eta)$, where $u(\alpha)$ has components $(\cos\alpha,\sin\alpha)$. The reception radius is unknown within [1000,1500] m, so the admissible sector ring is

$$F_1(R)=\left\{\rho u(\hat{\theta}_1+\eta):r_0<\rho\le R,|\eta|\le\delta\right\} \tag{3}$$

With $r_0=20$ m excluding the proximity case. The station at $S_2=bu(\hat{\theta}_1+\varphi)$ gives, by the law of cosines,

$$d_2(b,\varphi;\rho,\eta)=\sqrt{\rho^2+b^2-2\rho b\cos(\varphi-\eta)} \tag{4}$$

And the intersection angle γ at the source satisfies

$$|\sin\gamma|=\frac{b|\sin(\varphi-\eta)|}{d_2},\qquad \cos\gamma=\frac{\rho-b\cos(\varphi-\eta)}{d_2} \tag{5}$$

What governs accuracy is the lateral component $b|\sin(\varphi-\eta)|$, not the baseline: as $|\varphi-\eta|$ approaches 0 or π the lines become collinear and a small error produces large uncertainty, whereas an excessive lateral component pushes d_2 beyond the reception radius (Fig. 3).

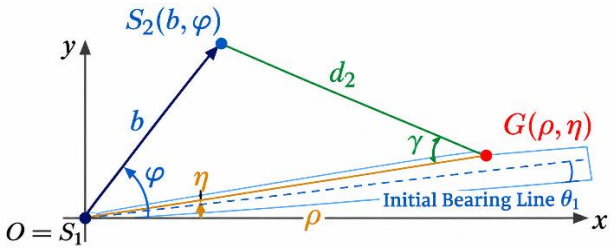

Figure 3. Sector ring after the first observation, station parameterization and intersection geometry

The value of d_2 separates three physical states:

$$L_D(b,\varphi;\rho,\eta,R)=\begin{cases}0, & d_2\le 20,\\ \max_{e_2\in[-\delta,\delta]} D\left(P_1\cap W\left(S_2,\hat{\theta}_2+e_2,\delta\right)\cap B\left(S_2,1500\right)\right), & 20<d_2\le R,\\ D_1, & d_2>R\end{cases} \tag{6}$$

Here P_1 is the feasible set from the first bearing, W the sector of a second bearing with error e_2, and $B(S_2,1500)$ the reception disk at the maximum radius. The first state is proximity confirmation with no residual uncertainty; the second takes the worst diameter over the unknown second error; the third receives nothing and falls back to $D_1=1500$ m, keeping the loss in units of length.

3.2. Area-Weighted Prior and Worst-Case Envelope

A uniform prior over area inside the ring gives the sector area

$$A_F(R)=\int_{-\delta}^{\delta}\int_{r_0}^{R}\rho\,\mathrm{d}\rho\,\mathrm{d}\eta=\delta\left(R^2-r_0^2\right) \tag{7}$$

So the radial weight is proportional to ρ rather than constant: a ring of fixed width covers more source positions as the radius grows, and a uniform range prior would understate the risk of distant sources. Discretizing into polar cells of exact area and taking each weight $w_{jk}(R)$ as its share of $A_F(R)$, the expected risk is

$$J_R(b,\varphi)=\sum_{j,k}w_{jk}(R)L_D(b,\varphi;\rho_j,\eta_k,R) \tag{8}$$

Normalized by D_1; since $0\le L_D\le D_1$ the result reads as the fraction of initial uncertainty surviving the second measurement.

The radius of a source is fixed while the agent knows only its interval, so it is treated as an interval parameter[10], discretized at 50 m into 11 scenarios. The robust risk and reliability indices are

$$J_{\max}(b,\varphi)=\max_{R\in\mathrm{R}} J_R(b,\varphi) \tag{9}$$

$$p_{\min}(b,\varphi)=\min_{R\in\mathrm{R}} p_{\mathrm{succ}}(b,\varphi;R) \tag{10}$$

Where the three masses sum to one; one index measures worst-case accuracy and the other worst-case availability.

$$p_{\mathrm{succ}}=p_{\mathrm{clr}}+p_{\mathrm{dir}}=1-p_{\mathrm{ns}},$$

3.3. Lexicographic Model and Near-Optimal Region

The decision is lexicographic in risk and baseline,

$$\min_{b,\varphi}\left(J_{\max}(b,\varphi),b\right)_{\mathrm{lex}}\quad \text{s.t.}\quad 0\le b\le 1800,\ -\pi\le\varphi\le\pi,\ p_{\min}(b,\varphi)\ge p_0 \tag{11}$$

With $p_0 = 0.95$. A weighted sum $J_{\max} + \lambda b$ would need an exchange rate between a metre of error and a metre of travel, which has no objective basis. The domain is symmetric about the first sight line, so a half-domain search on a 36 × 36 grid of 50 m × 5° cells, refined at 10 m/0.5°, 1 m/0.2° and 0.25 m/0.05°, suffices, with $\Delta\rho = 1$ m, $\Delta\eta = 0.25^\circ$, $\Delta e_2 = 0.125^\circ$ and $\Delta R = 50$ m, and the reception disk taken as a circumscribed 512-gon.

The result is $b^* = 1087.25$ m and $\varphi^* = \pm 30.15^\circ$, with $J^* = 59.941$ m and $p_{\min^*} = 0.989889$; the sign indicates mirror symmetry. Figure 4 shows the candidate region on the left and the risk contours with the $p_{\min} = 0.95$ boundary on the right. The offset is not the idealized 90°: perpendicular sight lines maximize the intersection angle, yet the second distance grows with the offset, reception failure becomes likelier and distant sources carry more area weight, so the compromise lands near 30°. At the optimum the second reading carries nearly all successful localizations, proximity confirmation is negligible and no-signal cases appear only at small radii. Across the eleven radius scenarios the expected risk is lowest near $R \approx 1100$ m and rises slowly beyond it, the 1500 m scenario being the worst. Table 1 sets the solution beside three reference strategies.

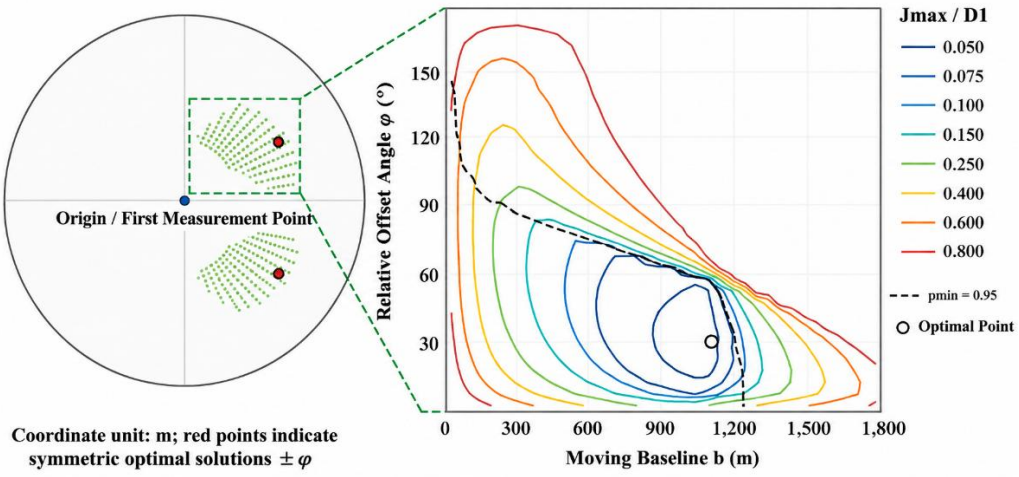

Figure 4. Risk contours, reliability boundary and near-optimal candidate region

Table 1. Worst-Case Comparison between the Optimal Scheme and Three Reference Strategies

Proposed	1087.25	30.15	59.941	0.989889
Along the line of sight	890.00	0.00	596.324	1.000000
Perpendicular move	221.00	90.00	358.657	0.951587
No movement	0.00	0.00	1500.000	1.000000

Moving along the sight line leaves the intersection angle near zero and the risk an order of magnitude higher, so extending it carries almost no information; the perpendicular move has an ideal angle but lowers the share of sources yielding a reading, so reliability falls to 0.951587. Staying put returns exactly D_1, matching the no-signal state. Against the initial scheme at $b = 1000$ m and $\varphi = 60^\circ$ with risk 80.418 m the reduction is 25.46%, and against staying put 96.00%.

A single optimum is sensitive to grid step, so execution needs a region of comparable performance:

$$C_{\tau,p_0} = \left\{ S_2(b,\varphi) : p_{\min}(b,\varphi) \geq p_0, \frac{J_{\max}(b,\varphi)}{D_1} \leq \frac{J^*}{D_1} + \tau \right\} \tag{12}$$

Table 2 relates the tolerance to the area, with the share taken against $\pi \cdot 1800^2$. Raising τ from 0.01 to 0.10 multiplies the area by about 4.4, and the reference $\tau = 0.05$ keeps 9.6193% of the disk.

Table 2. Tolerance against the Extent of the Candidate Region

τ	Risk threshold/m	Candidate area/m²	Share of target disk/%
0.010	74.9408	286015.83	2.8099
0.025	97.4408	647080.82	6.3572
0.050	134.9408	979129.71	9.6193
0.100	209.9408	1255328.06	12.3328

3.4. Sensitivity and Marginal Return

Four stress factors define a Sobol–Morris experiment: reception radius $R \sim U(1000,1500)$, error bound $\delta \sim U(0.5^\circ, 1.5^\circ)$, range lower bound $r_0 \sim U(5,20)$ and radial weight exponent $k \sim U(0,2)$ [11]. Variance decomposition ranks δ first on both indices. The reception radius has a first-order index of 0.1317 and a total index of 0.2658, so its influence runs mainly through interaction, and r_0 contributes little. At equal cost, tightening bearing accuracy lowers worst-case risk more than enlarging the radius, whose value is a constraint on availability.

Repeating the measurement updates the set by intersection,

$$P_{m+1} = P_m \cap H_{m+1} \tag{13}$$

With no historical constraint discarded. The sequence is

nested, so $D(P_{m+1}) \le D(P_m)$ and the expected error does not increase for any true position, error sequence and outcome, with or without the envelope. Monotonicity excludes deterioration but not a gain at each step: a station near an old one, or two nearly parallel sight lines, makes the new constraint nearly redundant. Under balanced placement and independent errors it falls at the $m^{-1/2}$ scale, and 20000 Monte Carlo replications drop the mean feasible diameter from 1500 m below the 40 m engineering threshold by the third observation, then flatten. Diminishing return gives the stopping rule: when the expected reduction no longer offsets travel and measurement cost, measurement stops and removal begins.

4. Seven-Point Coverage Search and Rolling-Horizon Scheduling

4.1. Analytic Detection Ring

The origin covers the central region of radius 1000 m, leaving the annulus $1000 < \rho \le 1800$ to m equiangular stations of radius a. The most adverse position lies on the bisector between neighbours, at distance

$$d^2 = 1800^2 + a^2 - 2 \cdot 1800 \cdot a \cos\frac{\pi}{m} \tag{14}$$

A convex quadratic in a minimized at $a = 1800\cos(\pi / m)$, where the worst distance is $1800\sin(\pi / m)$; coverage therefore requires

$$1800 \sin\frac{\pi}{m} \le 1000 \tag{15}$$

That is $\sin(\pi / m) \le 5/9$. Integers 2 to 5 fail and $m = 6$ succeeds first, giving a hexagon and, with the origin, seven points (Fig. 5). The seam and the rim impose $a \le 1732.05$ m and $1122.96 \le a \le 1994.74$ m, intersecting at [1122.96,1732.05] m. Margin rises with a while sweep length grows, the front peaks at $a = 1558.85$ m and shows a knee near $a \approx 1346.71$ m; rounding to $a = 1400$ m right of the knee leaves the worst position 913.91 m from its station, a margin of 86.09 m that absorbs coordinate rounding and the lower radius bound.

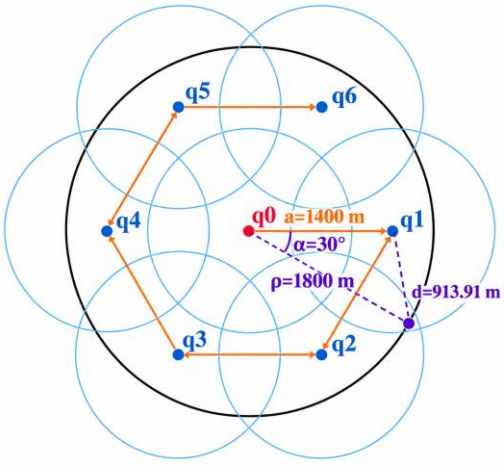

Figure 5. Guaranteed reception disks of the seven-point structure and the alternating visiting order

4.2. Coverage-Exclusion Screening and Removal Criterion

Of the 20 bands, 10 to 16 are occupied and the rest must be shown empty. If a band returns no signal at all seven stations and the seven disks cover the disk, it carries no source, so emptiness is falsifiable rather than a record of not having found anything. A direction reading marks a band occupied, a proximity return leads to removal, and no signal excludes the 1000 m disk around the station; adjacent stations scan bands in alternating directions to cut switches. Either of two equalities ends the search, $N_f = 16$, $N_f + N_e = 20$, the first marking the source ceiling and the second every band decided, while the task finishes only when $N_c = N_f$.

Removal requires the agent within 20 m of an unknown source, so the criterion is read from the set: with worst distance $r(c) = \max_{x \in P_h} d(x, c)$, the minimum enclosing radius $r_h = \min_c r(c)$ decides. When $r_h \le 20$ m, moving to the centre puts every admissible position within range without a point estimate. Otherwise the farthest pair approximates the long axis, candidates $q = C_h \pm d\, n_h$ are placed perpendicular to it subject to $\max_{x \in P_h} d(q, x) \le 1000$ m, and the choice minimizes $J(q) = w_1 T(q) + w_2 r_{\text{new}}(q)$, where $T(q)$ is the time to reach the candidate and measure, $r_{\text{new}}(q)$ the enclosing radius expected afterwards, and w_1 and w_2 the weights placed on travel and accuracy. The second station is kept as a candidate on equal terms, and a candidate serving several bands is shared, since only travel is shared.

4.3. Open-Route Dynamic Programming and Rolling Horizon

Up to 16 targets may satisfy the removal condition together, and enumerating orders costs $n!$, so open-route dynamic programming solves it exactly in $O(n^2 2^n)$ [12] with

$$c_{ij} = \frac{d(i, j)}{5} + 5 \tag{16}$$

The first term being travel and the second confirmation plus removal. With $F(S, j)$ the shortest time to visit S and stop at j,

$$F(S, j) = \min_{i \in S, i \ne j} \left[F(S \setminus \{j\}, i) + c_{ij} \right] \tag{17}$$

And $F(\{j\}, j) = c_{0j}$; no return to the start is required, so the route time is $\min_j F(S, j)$ and the sequence follows from the stored predecessors.

A sequence computed once applies to information that has since changed. The rolling horizon executes only the first step, reads the outcome, updates the sets and the remaining task, and solves again, dispatching on the current state: proximity to removal, a resolved target to the open route, an unresolved one to refinement, an incomplete discovery to the remaining stations. Total virtual time is

$$T = \frac{L}{5} + 5N_m + N_s + 5N_c \tag{18}$$

With L travel, N_m measurements, N_s switches and N_c removals, which puts search, refinement and removal on one scale. Table 3 reports six runs: per-source time varies with layout and discovery order while runtime stays small, so the algorithm is not the bottleneck.

Table 3. Simulated Runs for Omnidirectional and Mixed Sources

Scenario	Run	Sources removed	Mean time per source/s	Runtime/s
Omnidirectional	1	13	470.402	0.438
Omnidirectional	2	16	373.250	0.266
Omnidirectional	3	11	498.947	0.235
Mixed	1	11	861.391	2.375
Mixed	2	15	652.269	5.078
Mixed	3	10	1005.718	3.594

4.4. Dispersion–Time Regression

Using minimum spanning tree length as a dispersion index, six levels raise the mean normalized index from 962.5 m to 2761.0 m while mean per-source time rises from 373.6 s to 524.4 s. A linear fit gives

$$T = 299.791 + 0.08172\delta_{\mathrm{MST}}, \qquad R^2 = 0.9914 \tag{19}$$

With a Pearson correlation of 0.9957, so the index explains about 99% of the variance when the layout is unknown. The relation is an ex-ante estimate for omnidirectional sources only; the mixed scenario removes 36 sources with a source-count-weighted mean of 814.348 s and a range of 353.449 s, and half the sources need a detour, which blurs the trend.

5. Mixed Omnidirectional and Directional Sources

An omnidirectional source radiates uniformly, so availability depends on distance alone; a directional source radiates into a half-plane, so availability depends on bearing too, and behind the source no signal arrives however close the agent gets. The difference invalidates coverage arguments that rest on distance.

5.1. Inner-Outer Polygons and Reliability Screening

When a directional source sits on the target circle and radiates outward, every station inside lies behind it, so breaking the blind zone requires stations on the circle looking inward at the source from outside. The inner seven are kept and an outer regular polygon is added with vertices

$$q_k^{\mathrm{out}} = R_\Omega\left(\cos\left(\eta + \frac{2\pi k}{m}\right), \sin\left(\eta + \frac{2\pi k}{m}\right)\right), \qquad k = 0,1,\ldots,m-1 \tag{20}$$

Of side count m and phase η. It must enclose the inner hexagon, so $R_\Omega \cos(\pi/m) \ge a$; with $R_\Omega = 1800$ m and $a = 1400$ m this gives $m \ge \pi / \arccos(1400/1800) \approx 4.62$, hence $m \ge 5$. The condition fixes the layer relation only. Gaps between neighbours sum to 2π, and the mean-value and Cauchy inequalities bound the largest gap by $2\pi/m$ and the sum of squared gaps by $4\pi^2/m$, with equality under equiangular spacing, so a regular polygon minimizes both.

More sides improve directional coverage but add stations and travel. For a design (m,η), let $Y_s(d) = 1$ when every source of case s is found and removed before termination and 0 otherwise, and K_d count successes over N_{va} cases. A finite sample can overstate reliability, so a one-sided bound is used:

$$L_{0.95}(d) = \begin{cases} 0, & K_d = 0, \\ B^{-1}\left(0.05; K_d, N_{\mathrm{va}} - K_d + 1\right), & K_d > 0 \end{cases} \tag{21}$$

With B^{-1} the Beta quantile, the Clopper–Pearson bound [13]. Designs reaching 0.95 enter the feasible set, within which the smallest mean per-source time is chosen.

5.2. Half-Plane Approach and Angular Coverage

A source at g with emission direction u radiates into the half-plane centred on u, so an agent receiving at p lies inside it, $(p-g)^{\mathsf{T}} u \ge 0$.

Along the approach $p(\xi) = g + (1-\xi)(p-g)$ for $0 \le \xi \le 1$,

$$\left[p(\xi) - g\right]^{\mathsf{T}} u = (1-\xi)(p-g)^{\mathsf{T}} u \ge 0 \tag{22}$$

Holds throughout, so the agent cannot slip into the rear blind zone by moving. A straight approach is safe from the valid half-plane; from behind the source no straight path obtains a signal, so the agent must first go round.

With m discovery points sorted in bearing about the source, let g_i be the successive bearing gaps, g_m the wrap-around gap closing the circle, and G the largest. When $G \le 180^\circ$ at least one point lies in the valid half-plane for every emission direction, since a 180° half-plane cannot fit inside a smaller gap. Over 105 random positions about 95.492% satisfy this, with the rate near 100% in the inner region and falling near the rim; a check over 12000 positions and 1440 emission directions at 0.25° steps agreed with the dot-product test in every case, so fixed stations cannot cover all boundary positions unconditionally (Fig. 6).

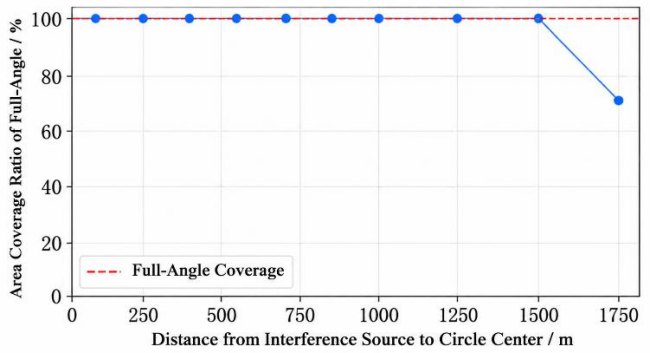

Figure 6. Share of positions with full angular coverage against distance from the centre

5.3. Tangential Blind Zone and Direction Estimation

A source on the circle radiating radially outward has $z = R_\Omega e_r$ and $u = e_r$, so every point x of the region satisfies

$$(x-z)^{\mathsf{T}} u = x^{\mathsf{T}} e_r - R_\Omega \le \| x\| - R_\Omega \le 0 \qquad (23)$$

And apart from the source itself no position inside the disk meets the reception condition, an outward tangential blind zone. Rotating the emission inward brings the measurable region inside: 90° gives 6.815% of the disk and 120° gives 9.387% (Fig. 7). The outer stations thus turn a certain miss into an event depending on phase, and a source between two stations emitting strictly outward can still be missed.

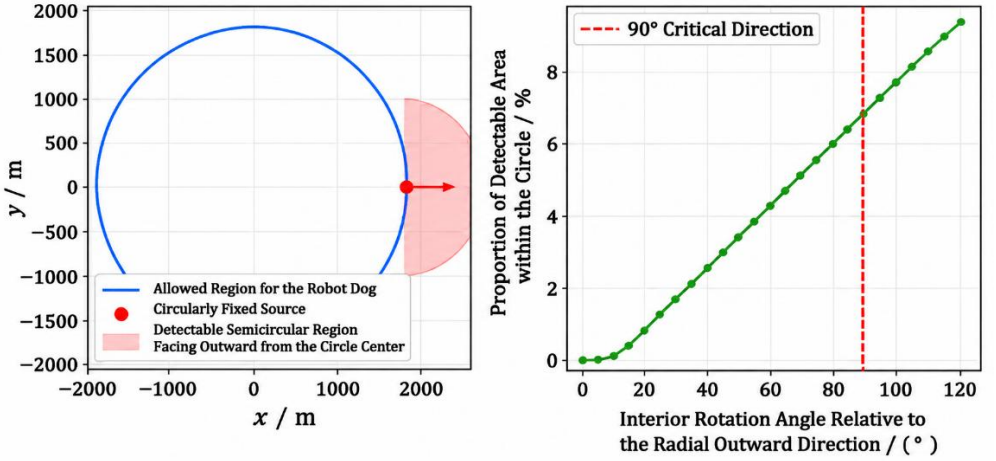

Figure 7. Outward tangential blind zone of a rim source and the measurable share after inward rotation

The emission direction follows from binary observations at equiangular probes. With $m \in \{3,4,6,8,12\}$ observations, position error standard deviations $\sigma_z \in \{0,10,20,40\}$ m and 5000 replications per combination, four probes show an angular degeneracy whose error exceeds that of three, since the symmetric layout yields two mirror solutions under the half-plane test. Apart from that case the error falls with more observations, reaching 7.575° mean absolute error with no position error and 12 observations, while $\sigma_z = 40$ m lowers the success rate to 79.12%.

6. Conclusions

The diameter of the feasible set and its covering property are separate conclusions. Rotating calipers bring the diameter search to linear time, yet the disk on the farthest pair leaves part of an equilateral-triangle region outside, so coverage is tested vertex by vertex and removal uses the minimum enclosing radius, not half the diameter.

Robust expected optimization places the three-state loss, the area-weighted prior and the radius envelope under one objective and, within a guaranteed success rate of 0.95, returns 1087.25 m, ±30.15° and 59.941 m, 25.46% below the initial scheme. The seven-point structure follows from the covering condition, the ring radius is set to 1400 m right of the Pareto knee with the worst position at 913.91 m, coverage exclusion makes emptiness falsifiable, and dynamic programming with a rolling horizon puts removal order and online updating on one scale. For mixed sources an outer polygon and a half-plane rule reduce the certain miss of outward radial emission to a phase-dependent probability.

Screening tasks with bounded errors, stationary targets and availability depending on distance and bearing are the natural fit, provided the error bound is stable, the prior is not far from the truth and the emission pattern falls into the omnidirectional or half-plane class; the reported schedules come from a discrete grid search and per-step replanning, so they are not globally optimal. Future work may replace the interval prior on the radius with a calibratable distribution and fold the synchronization cost of multiple agents into the same objective.

References

[1] Bishop, A. N., Fidan, B., Anderson, B. D. O., Doğançay, K., & Pathirana, P. N. (2010). Optimality analysis of sensor-target localization geometries. Automatica, 46(3), 479–492. https://doi.org/10.1016/j.automatica.2009.12.003

[2] Chen, Z., Zhang, S., Fang, Y., Fu, W., & Ji, M. (2025). The error lower bound of target state estimation in passive localization by bearing-only sensors. IEEE Transactions on Instrumentation and Measurement, 74, 1–14. https://doi.org/10.1109/TIM.2025.3551589

[3] Gu, Y., Sun, X., Zhu, B., & Cui, Y. (2026). Active localisation of intermittent radio frequency interference sources using an unmanned aerial vehicle in urban environments. IET Radar, Sonar & Navigation, 20(1). https://doi.org/10.1049/rsn2.70228

[4] Zhu, Y., Fang, X., & Li, C. (2025). Multi-sensor information fusion for mobile robot indoor-outdoor localization: A zonotopic set-membership estimation approach. Electronics, 14(5), 867. https://doi.org/10.3390/electronics14050867

[5] Jayalakshmi, K. P., Nair, V. G., & Sathish, D. (2025). A comprehensive survey on coverage path planning for mobile robots in dynamic environments. IEEE Access, 13, 60158–60185. https://doi.org/10.1109/ACCESS.2025.3556446

[6] Kuang, Y., Jiang, B., Cui, X., Li, S., Wang, J., & Song, H. (2024). Adaptive double-loop coverage optimization of underwater wireless directional restricted sensor networks. Ad Hoc Networks, 156, 103409. https://doi.org/10.1016/j.adhoc.2024.103409

[7] Fan, Y. A., & Liang, C. K. (2022). Hybrid discrete particle swarm optimization algorithm with genetic operators for target coverage problem in directional wireless sensor networks. Applied Sciences, 12(17), 8503. https://doi.org/10.3390/app12178503

[8] Wen, C., & Ma, H. (2024). An efficient two-stage evolutionary algorithm for multi-robot task allocation in nuclear accident rescue scenario. Applied Soft Computing, 152, 111223. https://doi.org/10.1016/j.asoc.2023.111223

[9] Preparata, F. P., & Shamos, M. I. (1985). Computational geometry: An introduction. Springer. https://doi.org/10.1007/978-1-4612-1098-6

[10] Ben-Tal, A., & Nemirovski, A. (2002). Robust optimization: Methodology and applications. Mathematical Programming, 92(3), 453–480. https://doi.org/10.1007/s101070100286

[11] Saltelli, A., Annoni, P., Azzini, I., Campolongo, F., Ratto, M., & Tarantola, S. (2010). Variance based sensitivity analysis of model output: Design and estimator for the total sensitivity index. Computer Physics Communications, 181(2), 259–270. https://doi.org/10.1016/j.cpc.2009.09.018

[12] Held, M., & Karp, R. M. (1962). A dynamic programming approach to sequencing problems. Journal of the Society for Industrial and Applied Mathematics, 10(1), 196–210. https://doi.org/10.1137/0110015

[13] Brown, L. D., Cai, T. T., & DasGupta, A. (2001). Interval estimation for a binomial proportion. Statistical Science, 16(2), 101–133. https://doi.org/10.1214/ss/1009213286